

Effect of transition metal doping on magnetic hardness of CeFe₁₂-based compounds

Justyn Snarski-Adamski* and Mirosław Werwiński
*Institute of Molecular Physics, Polish Academy of Sciences,
 M. Smoluchowskiego 17, 60-179 Poznań, Poland*

In this work, compositions of CeFe₁₁X and CeFe₁₀X₂ with all 3d, 4d, and 5d transition metal substitutions are considered. Since many previous studies have focused on the CeFe₁₁Ti compound, this particular case became the starting point of our considerations, and we gave it special attention. First, we determined the optimal symmetry of the simplest CeFe₁₁Ti structure model. Next, we observed that the calculated magnetocrystalline anisotropy energy (MAE) correlates with the magnetic moment, which in turn strongly depends on the choice of the exchange-correlation potential. MAE, magnetic moments, and magnetic hardness were determined for all compositions considered. Moreover, the calculated dependence of MAE on the spin magnetic moment allowed predicting the upper limits of the MAE. The compositions showing very high magnetic hardness include CeFe₁₁W, CeFe₁₀W₂, CeFe₁₁Mn, CeFe₁₀Mn₂, CeFe₁₁Mo, CeFe₁₀Mo₂, and CeFe₁₀Nb₂. Further alloying of selected compositions with elements embedded in interstitial positions confirms its positive effect on hard magnetic properties. Calculations carried out for comparison for selected isostructural La compounds lead to similar MAE results as those obtained for Ce compounds, suggesting a secondary effect of 4f electrons. Calculations were performed using the full-potential local-orbital electronic structure code FPLO18, whose unique fully relativistic implementation of the fixed spin moment method allowed the calculation of MAE dependence on magnetic moment.

I. INTRODUCTION

Rare-earth permanent magnets are used in industries such as automotive, aerospace, electronics, and renewable energy. They are alloys consisting mainly of transition metals and rare-earth elements. They have remarkable magnetic properties, such as very high energy density (BH)_{max} and the ability to operate at high temperatures. Of particular interest are rare-earth compounds such as Nd₂Fe₁₄B [1] and SmCo₅ [2] showing extremely high values of magnetocrystalline anisotropy. However, the high volatility of rare earth prices that became clearly evident during the so-called *rare-earth crisis* of 2011 [3] has mobilized the international research community to search for a new generation of hard magnetic materials with reduced rare-earth content [4–10]. These explorations, although mostly performed by experimental methods, are complemented by the efforts of groups conducting first-principles calculations of intrinsic properties and magnetic simulations at the microstructural level.

In the ongoing search for novel permanent magnets, special attention is being paid to magnetic compounds with ThMn₁₂-type structure based on Nd, Sm, but also less expensive Ce [11–15]. SmFe₁₁Ti and SmFe₁₁V systems were found to exhibit uniaxial magnetocrystalline anisotropy [15]. The Curie temperature (T_C) measured for SmFe₁₁V is equal to 361°C, the saturation magnetization is 11.2 kG (1.12 T), and the anisotropy field is 110 kOe [15].

The experimental MAE values for CeFe₁₁Ti range from 0.62 to 1.1 MJ m⁻³, and the magnetic moment (*m*) range from 21.2 to 22.5 μ_B f.u.⁻¹ [14, 16, 17]. Whereas,

TABLE I: Structural parameters of CeFe₁₂ (s.g. *I4/mmm*, No. 139). The lattice parameters are *a* = 8.539 and *c* = 4.78 Å, see Ref. [20].

Site	<i>x</i>	<i>y</i>	<i>z</i>
Ce (2 <i>a</i>)	0	0	0
Fe (8 <i>i</i>)	0.360	0	0
Fe (8 <i>j</i>)	0.265	0.5	0
Fe (8 <i>f</i>)	0.25	0.25	0.25

the exemplary MAE values for CeFe₁₁Ti obtained from first-principles calculations are equal to 1.19, 1.50, 1.57, and 1.98 MJ m⁻³ [17–19]. For CeFe₁₁Ti, the formation of a hard magnetic phase was also determined theoretically in the range from 700 K to 1100 K [13]. Furthermore, experimental analysis of Mo concentration in CeFe_{12-y}Mo_y, where *y* = 1, 1.5, and 2, showed that T_C for CeFe₁₁Mo is 421 K and decreases with Mo content, while for the nitrated counterpart T_C is 643 K [14]. The annealing, time-dependent value of (BH)_{max} takes the highest value for CeFe₁₁Mo equal to 0.3 MGOe.

The aim of this study is to theoretically determine the amount and type of dopants in CeFe₁₂ based alloys that will lead to maximizing their magnetic hardness. CeFe₁₁X and CeFe₁₀X₂ compositions (X = 3d, 4d, 5d elements) and, for comparison, the thermodynamically unstable CeFe₁₂ compound will be considered.

II. COMPUTATIONAL DETAILS

The calculations were performed using the full-potential local-orbital electronic structure code FPLO18 with a fixed atomic-like basis set [21]. The supercell method was used to model all the CeFe₁₁X and CeFe₁₀X₂

* Corresponding author: Justyn Snarski-Adamski
 justyn.snarski-adamski@ifmpan.poznan.pl

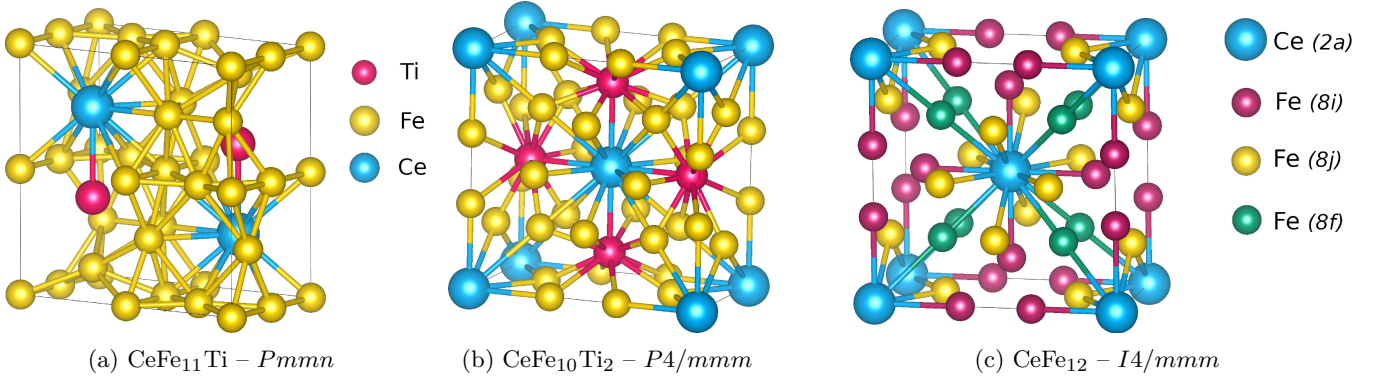


FIG. 1: Crystal structure models of (a) CeFe₁₁Ti (s.g. *Pmmn*, No. 59), (b) CeFe₁₀Ti₂ (s.g. *P4/mmm*, No. 123), and (c) CeFe₁₂ (s.g. *I4/mmm*, No. 139). CeFe₁₂ structure is a superstructure of the ThMn₁₂ type with *2a*, *8i*, *8j*, and *8f* Wyckoff positions. The lattice parameters of all models ($a = 8.539$, $c = 4.78$ Å) were adopted from Ref. [20].

systems ($X = 3d$, $4d$, and $5d$ elements). The generalized gradient approximation (GGA) was used in the Perdew-Burke-Ernzerhof (PBE) form [22]. The local spin density approximation (LSDA) in the von Barth and Hedin (BH) [23], Perdew and Zunger (PZ) [24], and Perdew and Wang (PW92) [25] forms was also used to analyze the effect of the exchange-correlation potential form on the magnetocrystalline anisotropy energy (MAE). It is found that a $12 \times 12 \times 12$ k-mesh leads to well converged MAE results. The density convergence criterion was set to 10^{-6} . In all cases, we optimized the geometry with a force convergence criterion of 10^{-3} eV Å⁻¹. Similar systematic supercell approach has been previously used to model the (Fe,Co,X)₂B [26] and (Fe,Co,X)₅PB₂ alloys [27].

CeFe₁₂ crystallizes in a tetragonal structure with space group *I4/mmm* [14, 15], see Table I and Fig. 1c. For all considered models, we assumed the lattice parameters like those measured for CeFe₁₂ [20], while the Wyckoff positions have been optimized using the spin-polarized scalar-relativistic approach. For CeFe₁₂, we optimize the atomic positions using various exchange-correlation functionals available in FPLO.

For CeFe₁₁Ti, we considered a number of the simplest supercell models and selected the structure with the lowest total energy (*Pmmn*), see Fig. 1a. In the case of CeFe₁₀Ti₂ there is only one possible crystallographic configuration with a space group *P4/mmm* (No. 123), see Fig. 1b. Tables with the evaluated atomic positions can be found in the Appendix. The VESTA code was used for visualization of crystal structures [28].

For the "1-10-2" tetragonal system, the MAE was determined as the difference between the fully relativistic total energies calculated for [100] and [001] quantization axes. For "1-11-1" system, the MAE was evaluated as the difference between the energies calculated for the orthogonal [101] and [010] axes. We chose the unconventional [101] axis because the space group under consideration (*Pmmn*, No. 59) is orthorhombic. We interpret the energy value obtained for [101] axis as the value averaged

between axes [100] and [001]. In the adopted sign convention, the positive sign of the MAE is consistent with an easy magnetization axis along the [010] direction, and the negative sign is consistent with in-plane anisotropy. Furthermore, we determined MAE values from single iteration fully-relativistic approach. Using the fully relativistic fixed spin moment scheme [29], we also study MAE as a function of the total spin magnetic moment (m_S).

Another important parameter in the context of permanent magnets is magnetic hardness, defined as:

$$\kappa = \sqrt{\frac{|K|}{\mu_0 M_S^2}}, \quad (1)$$

where K is the magnetocrystalline anisotropy constant, M_S is the saturation magnetization, and μ_0 is vacuum permeability. The empirical rule $\kappa > 1$ specifies whether the material will resist self-demagnetization [8]. In determining the theoretical value of κ , we assume that the anisotropy constant K is equal to MAE and M_S is evaluated based on the calculated total magnetic moment and unit cell volume. It is worth noting that magnetic hardness only makes sense in materials that are proper permanent magnets, and thus have a magnetization easy-axis rather than an easy-plane. Thus, when $\text{MAE} < 0$ (easy-plane anisotropy), the magnetic hardness parameter loses its meaning [30] and in our calculations is considered as zero.

III. RESULTS AND DISCUSSION

A. Magnetic properties of CeFe₁₂

Earlier calculations for CeFe₁₁Ti gave a rather large spread of MAE (from 1.19 to 1.98 MJ m⁻³) accompanied by a similarly large spread of magnetic moments (from 19.19 to 24.04 μ_B f.u.⁻¹) [17–19]. To confirm the conjecture that the obtained differences have their origin

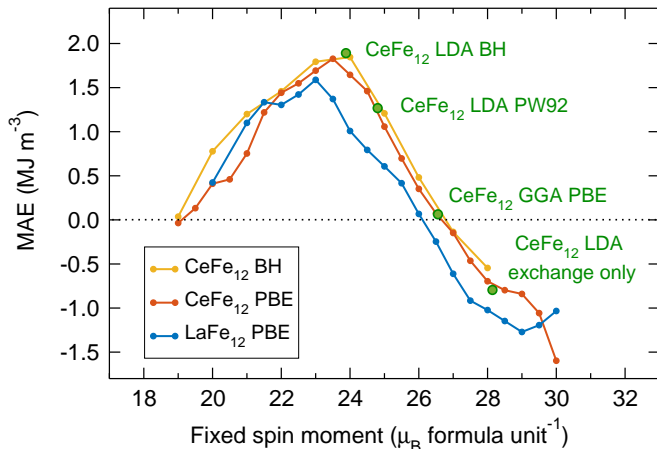


FIG. 2: The magnetocrystalline anisotropy energy (MAE) dependence of the fixed spin moment for CeFe_{12} calculated with von Barth-Hedin (BH) and Perdew-Burke-Ernzerhof (PBE) exchange-correlation potentials. Together with corresponding PBE results for LaFe_{12} and equilibrium values for CeFe_{12} obtained for various functionals. The calculations were performed using the FPLO18 code.

in the choice of the exchange-correlation potential, we performed MAE and magnetic moment calculations for the parent CeFe_{12} phase using the BH, PW92, PBE, and LDA exchange-only functionals. The results for various functionals are as follows: BH (MAE = 1.89 MJ m^{-3} , $m_S = 23.88 \mu_B \text{ f.u.}^{-1}$), PW92 (MAE = 1.27 MJ m^{-3} , $m_S = 24.80 \mu_B \text{ f.u.}^{-1}$), PBE (MAE = 0.06 MJ m^{-3} , $m_S = 26.56 \mu_B \text{ f.u.}^{-1}$), and LDA exchange only (MAE = -0.79 MJ m^{-3} , $m_S = 28.14 \mu_B \text{ f.u.}^{-1}$). As we can see, the range of MAE values obtained is huge, and they correlate with the values of magnetic moments. Looking at Fig. 2, it is easy to notice that these values lie on a common straight line, so we can say that the MAE correlates with the value of total spin magnetic moment (m_S).

Further insight into the observed relationship can be obtained thanks to the fully relativistic implementation of the fixed spin moment (FSM) method, which allows us to calculate the MAE as a function of total spin magnetic moment. The results of the MAE(m_S) calculation for the PBE functional confirm that the spin magnetic moment is the significant factor affecting the MAE value. Moreover, the MAE(m_S) calculation for another exchange-correlation functional (BH) confirmed that the result of MAE(m_S) does not depend on the choice of the functional itself. Hence, we conclude that the MAE(m_S) function is more universal fingerprint of the material than the equilibrium MAE values calculated for individual functionals.

The MAE(m_S) result for LaFe_{12} shown in the Fig. 2 will be addressed in the further part of this work dis-

TABLE II: Magnetic moments on Ce, Fe, Ti atoms in $\text{CeFe}_{11}\text{Ti}$ (s.g. $Pmmn$, No. 59), CeFe_{12} (s.g. $I4/mmm$, No. 139).

CeFe ₁₁ Ti s.g. <i>Pmmn</i>			CeFe ₁₂ s.g. <i>I4/mmm</i>		
Site	m_s	m_l	Site	m_s	m_l
Ce	-1.13	0.290	Ce	-1.11	0.227
Fe	1.70	0.036	Fe	2.57	0.069
Fe	1.86	0.039	Fe	2.38	0.056
Fe	2.47	0.059	Fe	1.96	0.039
Fe	2.23	0.058			
Fe	2.08	0.050			
Fe	2.33	0.049			
Fe	2.24	0.046			
Ti	-1.26	0.015			

TABLE III: The energy difference between the considered structure and the lowest energy structure $Pmmn$ [$E - E_0$ (meV)], the magnetocrystalline anisotropy energy [MAE (MJ m^{-3})], the spin magnetic moments on Ce [$m_s(\text{Ce})$] and Ti [$m_s(\text{Ti})$], orbital magnetic moment on Ti [$m_l(\text{Ti})$], total magnetic moment [m], and magnetic hardness [κ] calculated for different possible types of structures of $\text{CeFe}_{11}\text{Ti}$ compound. Magnetic moments are expressed in μ_B per atom of formula unit. Calculations were performed with FPLO18 using the PBE functional.

S.g.	$E - E_0$	MAE	$m_s(\text{Ce})$	$m_s(\text{Ti})$	$m_l(\text{Ti})$	m	κ
<i>Amm2</i>	31.2	1.14	-1.04	-1.24	0.014	22.01	0.81
<i>Ama2</i>	116.8	1.08	-1.01	-1.22	0.014	21.99	0.79
<i>Imm2</i>	39.8	1.15	-1.10	-1.26	0.014	21.92	0.82
<i>Pmmm</i>	344.6	1.02	-1.08	-1.26	0.010	22.50	0.75
<i>Pmmn</i>	0.0	1.00	-1.10	-1.30	0.015	21.24	0.79

cussing the influence of $4f$ electrons on MAE value. The plots for LaFe_{12} and CeFe_{12} are similar in shape. In both cases, a decrease in the equilibrium value of magnetic moment leads to an increase in MAE, which reaches maximum values 1.58 MJ m^{-3} for LaFe_{12} and 1.82 MJ m^{-3} for CeFe_{12} . In Table II, we are presenting the orbital and spin magnetic moments in CeFe_{12} compound.

B. Structural and magnetic properties of CeFe_{12} -based compounds with Ti

1. Supercell model of $\text{CeFe}_{11}\text{Ti}$

To prepare the simplest supercell to model the composition of $\text{CeFe}_{11}\text{Ti}$, we consider five possible non-equivalent configurations of substitutions of the dopant atom at the Fe ($8i$) position leading to a change in the space group of the resulting unit cells, see Fig. 3. These

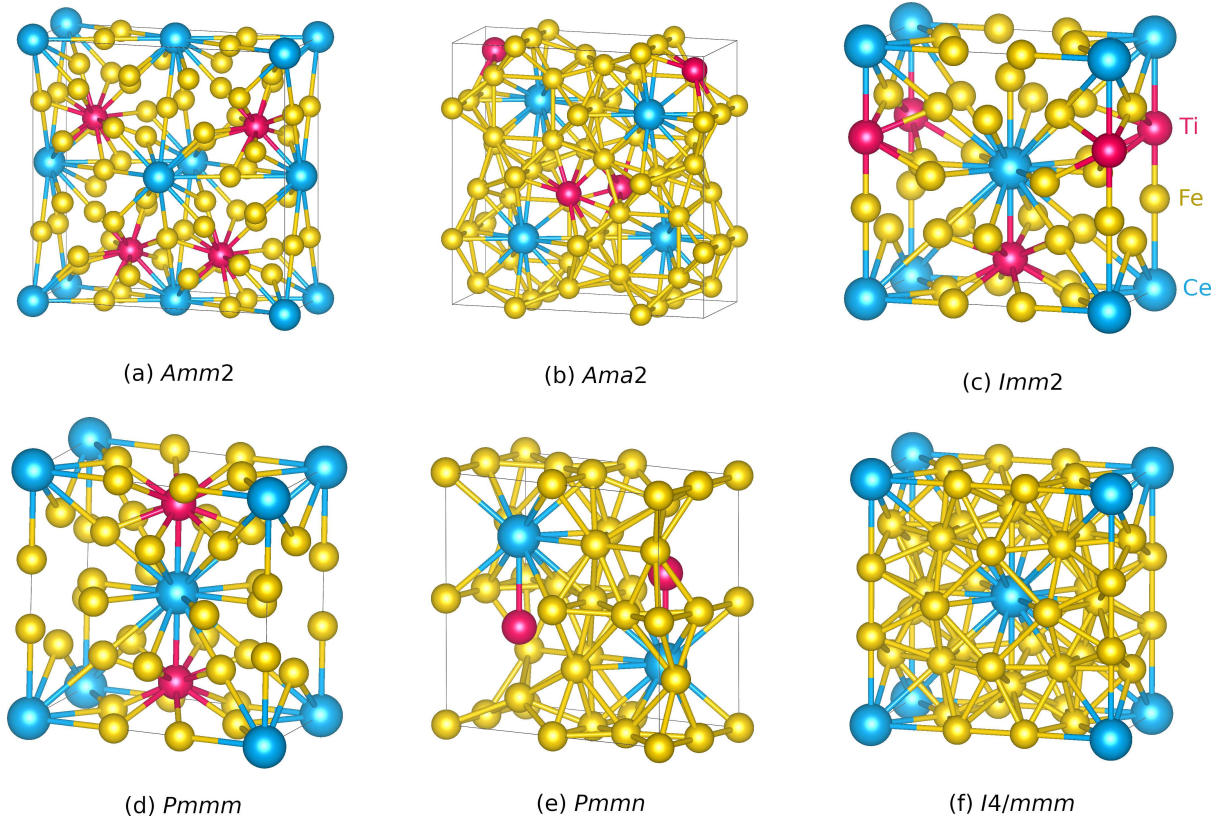


FIG. 3: (a–e) Five orthorhombic crystal structures prepared for $\text{CeFe}_{11}\text{Ti}$ compound and (f) tetragonal crystal structure for CeFe_{12} .

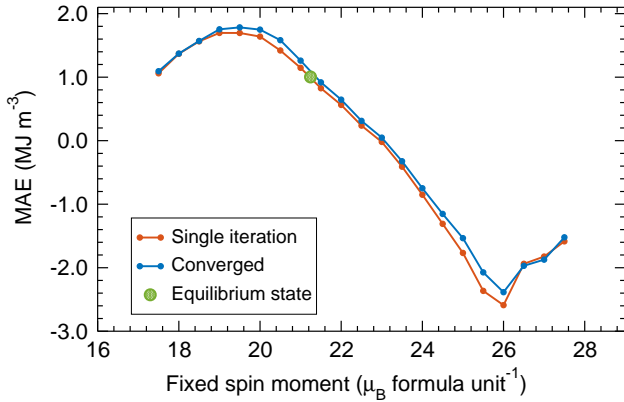


FIG. 4: Magnetocrystalline anisotropy energies (MAEs) as a function of fixed spin moment for the $\text{CeFe}_{11}\text{Ti}$ compound calculated using full-convergence method (blue line) and the method using a single fully relativistic iteration (orange line). The green point represents the equilibrium value. The calculations were performed using FPLO18 with the PBE functional.

non-equivalent space groups are included in Table III, along with the individual MAEs, total and partial magnetic moments, and the energy difference relative to the

TABLE IV: Experimental values of magnetocrystalline anisotropy energy [MAE (MJ m^{-3})] for $\text{CeFe}_{11}\text{Ti}$ compound.

Technique	Ref.	MAE
X-ray diffraction	[16]	0.76
Magnetization curve	[14]	0.62
Magnetization curve	[17]	1.10

lowest energy structure ($E-E_0$). The cell with space group *Pmmn* has the lowest energy among the considered structures, so we choose it as the basic unit cell for the calculation of CeFe_{11}X compounds presented later in this paper. We identify the use of structures with space group *Imm2* in the earlier works [12, 13, 19, 31] as one of the factors which may lead to the differences between our and previous results. The range of MAE obtained for structures with different space groups is from 1.00 to 1.15 MJ m^{-3} and the corresponding range for total magnetic moment (m) is from 21.24 to $22.50 \mu_B \text{ f.u.}^{-1}$. To compare the obtained values for $\text{CeFe}_{11}\text{Ti}$, the experimental results using test techniques based on the magnetization curves and X-ray diffraction are presented in Table IV. We conclude that the presented calculated MAEs are in relatively good agreement with the experimentally obtained values.

TABLE V: Magnetocrystalline anisotropy energy [MAE (MJ m^{-3})], total magnetic moment [m ($\mu_B \text{ f.u.}^{-1}$)], and magnetic hardness [κ] for selected $\text{CeFe}_{12-y}\text{Ti}_y$ compounds. The calculations were performed with FPLO18 using the PBE functional.

Compound	S.g.	MAE	m	κ
CeFe_{12}	$I4/mmm$	0.06	26.55	0.16
$\text{CeFe}_{11.5}\text{Ti}_{0.5}$	$Pmm2$	0.59	24.68	0.52
$\text{CeFe}_{11}\text{Ti}$	$Pmmn$	1.00	21.24	0.79
$\text{CeFe}_{10}\text{Ti}_2$	$P4/mmm$	1.30	18.04	1.06

We can see in Table III that the spin magnetic moment on the Ce atom is in all cases close to $-1 \mu_B$. A negative sign in this notation means the opposite magnetization to the ferromagnetic matrix of Fe. In the case of $Pmmn$ structure, spin and orbital magnetic moments on the Ce, Fe, and Ti have been shown in Table II.

2. Effect of Ti concentration on magnetic properties

Comparing the presented computational results for CeFe_{12} and $\text{CeFe}_{11}\text{Ti}$, we predict that further increase of the amount of substituent should lead to a decrease in the total magnetic moment, which, due to the $\text{MAE}(m)$ relation, should lead to an increase in the MAE value. These predictions are tentatively confirmed by the results for $\text{CeFe}_{12-y}\text{Ti}_y$, where $y = 0, 0.5, 1, 2$, presented in Table V. We can see, that the magnetic moment strongly decreases with increasing concentration of Ti, and we observe a close to linear dependence of $\text{MAE}(y)$. We can also see that for $y = 2$ the result of magnetic hardness is clearly above 1, which makes this material a potential new permanent magnet.

3. Fixed spin moment calculations

Figure 4 presenting the $\text{MAE}(m_S)$ relation for $\text{CeFe}_{11}\text{Ti}$ is very similar to the analogous result for CeFe_{12} shown earlier, see Fig. 2. In both cases, we observe a parabola-shaped relationship with a maximum below the equilibrium magnetic moment. For $\text{CeFe}_{11}\text{Ti}$, the MAE maximum of 1.78 MJ m^{-3} occurs for a total spin magnetic moment of $19.5 \mu_B \text{ f.u.}^{-1}$, while the equilibrium MAE value is 1.00 MJ m^{-3} for $m_S = 21.2 \mu_B \text{ f.u.}^{-1}$. Comparing again the results for $\text{CeFe}_{11}\text{Ti}$ and CeFe_{12} , we can interpret the increase in the equilibrium MAE value for $\text{CeFe}_{11}\text{Ti}$ as the effect of the reduction of the total magnetic moment of the system induced by doping. Furthermore, a comparison of the fully convergent calculations shown in Fig. 4 with calculations based on a single fully relativistic iteration positively verifies the approximation, which main benefit is the multiple computation time reduction.

4. Effect of interstitial dopants on magnetic hardness

TABLE VI: The magnetocrystalline anisotropy energy [MAE (MJ m^{-3})], total magnetic moment [m ($\mu_B \text{ f.u.}^{-1}$)], and magnetic hardness [κ] for CeFe_{12} -based and $\text{CeFe}_{11}\text{Ti}$ -based compounds with interstitial dopants H, B, C, and N. The calculations were performed with the FPLO18 code using the PBE functional.

Compound	MAE	m	κ
CeFe_{12}	0.06	26.55	0.16
CeFe_{12}H	1.12	25.83	0.69
CeFe_{12}C	1.50	25.39	0.81
CeFe_{12}N	1.82	27.03	0.84
$\text{CeFe}_{11}\text{Ti}$	1.00	21.24	0.79
$\text{CeFe}_{11}\text{TiB}$	1.52	20.96	0.99
$\text{CeFe}_{11}\text{TiN}$	1.64	22.53	0.95

To shift the position on the $\text{MAE}(m_S)$ curve from the equilibrium location toward the observed maximum, we consider adding light atoms such as carbon, nitrogen, or hydrogen in the interstitial positions of CeFe_{12} and $\text{CeFe}_{11}\text{Ti}$. From the results presented in Table VI, we see that nitriding allows us to approach the maximum MAE value for the pure CeFe_{12} compound. The results for $\text{CeFe}_{11}\text{TiB}$ and $\text{CeFe}_{11}\text{TiN}$ show that doping with a light atom can increase both the MAE value and the magnetic hardness of the resulting compound.

C. Intrinsic magnetic properties of CeFe_{11}X and $\text{CeFe}_{10}\text{X}_2$ compounds

1. Magnetocrystalline anisotropy energy

Since we considered the doping of CeFe_{11}X and $\text{CeFe}_{10}\text{X}_2$ with all $3d$, $4d$, and $5d$ transition metals, we obtained a complete picture of the MAE changes with the type and amount of substituted transition metals, see Figs. 5a and 5d and Table VII. A similar course has been shown before for alloys $(\text{Fe}, \text{Co}, \text{X})_5\text{PB}_2$ substituted with $5d$ transition metal [27]. Moreover, the dependence of magnetic hardness (κ) on transition metals is shown in Figs. 5b and 5e. We can see that the magnetic hardness results are similar to the MAE trends. Among all CeFe_{11}X compositions, only $\text{CeFe}_{11}\text{Nb}$ and $\text{CeFe}_{11}\text{Re}$ could be classified as hard permanent magnets ($\kappa > 1$), while the values of κ for CeFe_{11}W and $\text{CeFe}_{11}\text{Mo}$ are slightly below the classification criterion, which is still a good indication for further modifications.

In the context of potential applications, besides the physical parameters, the economic aspect must be taken into account. Thus, although we observe that Au and Pt significantly increase magnetic hardness, it is difficult to imagine their practical applications. Taking into account the raw material prices, the economically feasible

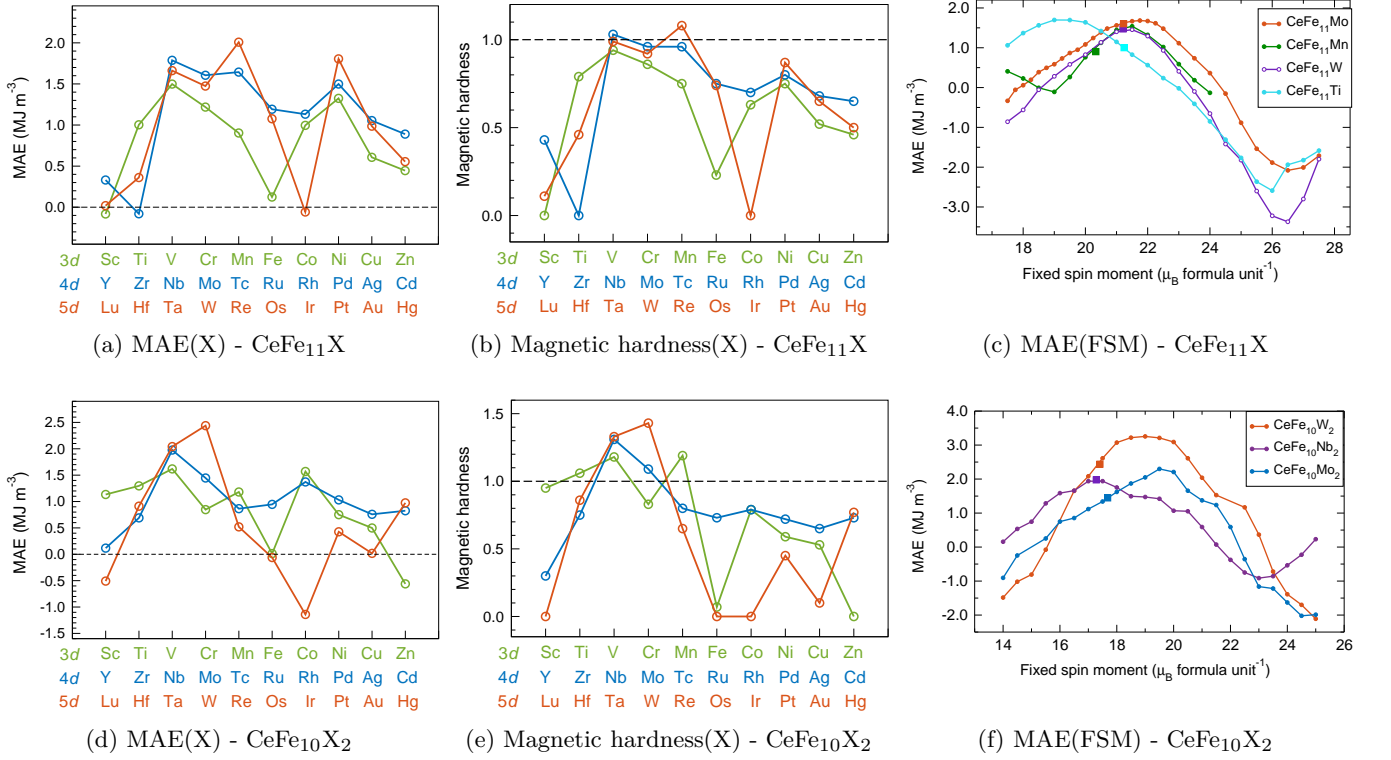


FIG. 5: The hard-magnetic properties of CeFe₁₁X and CeFe₁₀X₂ systems calculated for various 3d, 4d, and 5d transition metals. (a, d) the magnetocrystalline anisotropy energy, (b, e) the magnetic hardness, and (c, f) magnetocrystalline anisotropy energy dependencies of fixed spin moment for the selected elements (X = Mo, Mn, W, Ti for CeFe₁₁X and X = W, Nb, Mo for CeFe₁₀X₂). The squares in the MAE(FSM) plots represent equilibrium values. The calculations were performed with FPLO18 using the PBE functional and supercell approach.

group of dopants will include Ti, Cr, Ni, W, Mo, Mn, and Nb. The MAE(m_S) dependencies for the selected "1-11-1" system are shown in Fig. 5c and calculated for the Ti, W, Mo, and Mn dopants, indicating that in each of these cases the CeFe₁₁X compound has the potential to reach the MAE of about 1.5 MJ m⁻³, followed by $\kappa > 1$.

Calculations of the MAE of CeFe₁₀X₂ compositions show that the compounds: CeFe₁₀W₂, CeFe₁₀Nb₂, CeFe₁₀Mo₂, and CeFe₁₀Mn₂ could be classified as hard permanent magnets and can be worth further investigations. For selected compounds, we have also calculated FSM curves to show that, especially in the case of the CeFe₁₀W₂ compound, there is a possible range for further modification to obtain a very high value of MAE above 3 MJ m⁻³, see Fig. 5f.

2. Magnetic moments

The results presented in Figs. 6b and 6e clearly show that the substitution of the aforementioned elements in the position 8i lowers the spin magnetic moment of all considered compositions in relation to the parental CeFe₁₂ compound. For doping with Mn we observe the smallest values of both the total spin magnetic moment

and the partial magnetic moment. We further observe that the function of orbital and spin magnetic moments on substitutions resembles the waveform of the sine function with a minimum and maximum on the positive and negative side of the value interval, see Fig. 6. For considered CeFe₁₁X compounds, the range of spin magnetic moments on Ce atom is from -0.88 to -1.15 μ_B , and the orbital magnetic moments on Ce atom is from 0.14 to 0.31 μ_B . The results obtained are consistent with previous calculations of the dependence of the total spin magnetic moment on the position of substitution using the example of the 3d elements in NdFe₁₁X system [32]. Analogous trends in the substitution of 5d elements in 3d matrix have previously been found computationally [27, 33, 34] and experimentally [35].

3. Effect of 4f electrons on magnetocrystalline anisotropy

In the heavy fermion regime, the local magnetic moment of Ce is shielded by conduction electrons that couple to a single Ce 4f electron to form a nonmagnetic single state [31]. This kind of heavy-fermionic behavior of Ce has been observed in families "1-5" (CeCo₅) [36] and "2-14-1" (Ce₂Fe₁₄B) [37] of hard-magnetic inter-

TABLE VII: The magnetocrystalline anisotropy energy [MAE (MJ m^{-3})], total magnetic moment [m], magnetic hardness [κ], orbital magnetic moment [$m_l(\text{X})$], and spin magnetic moment [$m_s(\text{X})$] calculated for various 3d, 4d, and 5d transition metal elements X in compounds CeFe_{11}X (s.g. $P6mm$, No. 59) and $\text{CeFe}_{10}\text{X}_2$ (s.g. $P4/mmm$, No. 123). Magnetic moments are expressed in μ_B per atom of formula unit. Calculations were performed with FPLO18 using the PBE functional.

CeFe_{11}X						$\text{CeFe}_{10}\text{X}_2$					
3d elements											
	MAE	m	κ	m_l	m_s		MAE	m	κ	m_l	m_s
$\text{CeFe}_{11}\text{Sc}$	-0.08	22.37	0.00	-0.002	-0.71	$\text{CeFe}_{10}\text{Sc}_2$	1.13	18.80	0.95	-0.003	-0.68
$\text{CeFe}_{11}\text{Ti}$	1.00	21.24	0.79	0.015	-1.30	$\text{CeFe}_{10}\text{Ti}_2$	1.30	18.04	1.06	0.011	-1.15
CeFe_{11}V	1.50	21.75	0.94	0.036	-2.00	$\text{CeFe}_{10}\text{V}_2$	1.62	18.06	1.18	0.028	-1.15
$\text{CeFe}_{11}\text{Cr}$	1.22	21.51	0.86	0.034	-2.91	$\text{CeFe}_{10}\text{Cr}_2$	0.85	18.51	0.83	0.024	-1.33
$\text{CeFe}_{11}\text{Mn}$	0.90	21.14	0.75	-0.003	-3.15	$\text{CeFe}_{10}\text{Mn}_2$	1.18	15.29	1.19	0.002	-2.82
$\text{CeFe}_{11}\text{Fe}$	0.12	26.12	0.23	0.053	2.64	$\text{CeFe}_{10}\text{Fe}_2$	0.01	27.30	0.07	0.048	2.38
$\text{CeFe}_{11}\text{Co}$	1.00	26.38	0.63	0.107	1.52	$\text{CeFe}_{10}\text{Co}_2$	1.57	26.47	0.79	0.109	1.60
$\text{CeFe}_{11}\text{Ni}$	1.32	25.87	0.75	0.082	0.57	$\text{CeFe}_{10}\text{Ni}_2$	0.75	24.42	0.59	0.081	0.57
$\text{CeFe}_{11}\text{Cu}$	0.61	25.15	0.52	0.019	-0.06	$\text{CeFe}_{10}\text{Cu}_2$	0.50	22.32	0.53	0.013	-0.08
$\text{CeFe}_{11}\text{Zn}$	0.45	24.07	0.46	0.000	-0.27	$\text{CeFe}_{10}\text{Zn}_2$	-0.56	20.51	0.00	0.000	-0.24
4d elements											
	MAE	m	κ	m_l	m_s		MAE	m	κ	m_l	m_s
CeFe_{11}Y	0.33	22.39	0.43	0.000	-0.45	$\text{CeFe}_{10}\text{Y}_2$	0.12	19.26	0.30	0.000	-0.46
$\text{CeFe}_{11}\text{Zr}$	-0.08	21.72	0.00	0.010	-0.80	$\text{CeFe}_{10}\text{Zr}_2$	0.69	18.62	0.75	0.004	-0.54
$\text{CeFe}_{11}\text{Nb}$	1.79	21.77	1.03	0.020	-1.07	$\text{CeFe}_{10}\text{Nb}_2$	1.98	17.98	1.31	0.013	-0.60
$\text{CeFe}_{11}\text{Mo}$	1.61	22.06	0.96	0.014	-1.02	$\text{CeFe}_{10}\text{Mo}_2$	1.45	18.45	1.09	0.013	-0.61
$\text{CeFe}_{11}\text{Tc}$	1.64	22.30	0.96	-0.028	-0.64	$\text{CeFe}_{10}\text{Tc}_2$	0.86	19.55	0.80	0.002	-0.47
$\text{CeFe}_{11}\text{Ru}$	1.19	24.26	0.75	-0.022	0.19	$\text{CeFe}_{10}\text{Ru}_2$	0.95	22.25	0.73	-0.017	0.15
$\text{CeFe}_{11}\text{Rh}$	1.13	25.65	0.70	0.035	0.47	$\text{CeFe}_{10}\text{Rh}_2$	1.37	24.78	0.79	0.052	0.61
$\text{CeFe}_{11}\text{Pd}$	1.50	25.71	0.80	0.048	0.21	$\text{CeFe}_{10}\text{Pd}_2$	1.03	23.76	0.72	0.040	0.18
$\text{CeFe}_{11}\text{Ag}$	1.05	25.30	0.68	0.020	-0.08	$\text{CeFe}_{10}\text{Ag}_2$	0.76	22.32	0.65	0.011	-0.09
$\text{CeFe}_{11}\text{Cd}$	0.89	24.37	0.65	0.003	-0.25	$\text{CeFe}_{10}\text{Cd}_2$	0.83	20.81	0.73	0.001	-0.22
5d elements											
	MAE	m	κ	m_l	m_s		MAE	m	κ	m_l	m_s
$\text{CeFe}_{11}\text{Lu}$	0.02	22.08	0.11	0.013	-0.41	$\text{CeFe}_{10}\text{Lu}_2$	-0.51	19.18	0.00	0.020	-0.41
$\text{CeFe}_{11}\text{Hf}$	0.36	21.85	0.46	0.029	-0.74	$\text{CeFe}_{10}\text{Hf}_2$	0.91	18.58	0.86	0.014	-0.52
$\text{CeFe}_{11}\text{Ta}$	1.66	21.88	0.99	0.041	-1.02	$\text{CeFe}_{10}\text{Ta}_2$	2.04	17.97	1.33	0.020	-0.61
CeFe_{11}W	1.47	22.09	0.92	0.015	-0.95	$\text{CeFe}_{10}\text{W}_2$	2.44	18.26	1.43	0.010	-0.59
$\text{CeFe}_{11}\text{Re}$	2.01	22.00	1.08	-0.053	-0.71	$\text{CeFe}_{10}\text{Re}_2$	0.52	18.56	0.65	-0.027	-0.46
$\text{CeFe}_{11}\text{Os}$	1.08	23.56	0.74	-0.160	-0.08	$\text{CeFe}_{10}\text{Os}_2$	-0.06	20.67	0.00	-0.095	-0.16
$\text{CeFe}_{11}\text{Ir}$	-0.06	25.26	0.00	-0.036	0.29	$\text{CeFe}_{10}\text{Ir}_2$	-1.14	24.02	0.00	-0.017	0.35
$\text{CeFe}_{11}\text{Pt}$	1.80	25.89	0.87	0.079	0.25	$\text{CeFe}_{10}\text{Pt}_2$	0.43	24.24	0.45	0.081	0.24
$\text{CeFe}_{11}\text{Au}$	0.99	25.67	0.65	0.069	0.01	$\text{CeFe}_{10}\text{Au}_2$	0.02	22.97	0.10	0.047	-0.02
$\text{CeFe}_{11}\text{Hg}$	0.55	24.76	0.50	0.027	-0.17	$\text{CeFe}_{10}\text{Hg}_2$	0.97	21.36	0.77	0.015	-0.16

metallics. To determine the effect of 4f electrons on the obtained MAE values, we performed $\text{MAE}(m_S)$ calculations for an isostructural LaFe_{12} compound with an empty 4f shell, see Fig. 2. The relatively small differences observed between the $\text{MAE}(m_S)$ curves calculated for the LaFe_{12} and CeFe_{12} compounds indicate that, at least in the PBE approximation, the effect of the 4f shell on the MAE values is small. MAE calculations for $\text{LaFe}_{11}\text{Ti}$ (0.66 MJ m^{-3}), $\text{CeFe}_{11}\text{Ti}$ (1.00 MJ m^{-3}), $\text{LaFe}_{10}\text{W}_2$ (1.91 MJ m^{-3}), and $\text{CeFe}_{10}\text{W}_2$ (2.43 MJ m^{-3}) also confirm the secondary effect of the 4f shell on the MAE value in these compounds. Since La and Ce are extracted in large quantities during the mining of Nd-containing rare earth ores, both these elements can play an important role in the development of lower-cost high-

performance permanent magnets.

IV. SUMMARY AND CONCLUSIONS

Using density functional theory, we investigated the magnetic properties of the compounds CeFe_{11}X and $\text{CeFe}_{10}\text{X}_2$ with all 3d, 4d, and 5d transition metals. As a starting example, we used the $\text{CeFe}_{11}\text{Ti}$ system, for which we determined the simplest model of the crystal structure and further studied how the change of Ti concentration affects the obtained magnetic properties. We found that in the doping range of 0 to 2 Ti atoms per 12 Fe atoms, an increase in Ti concentration leads to a decrease in the total magnetic moment and to a significant

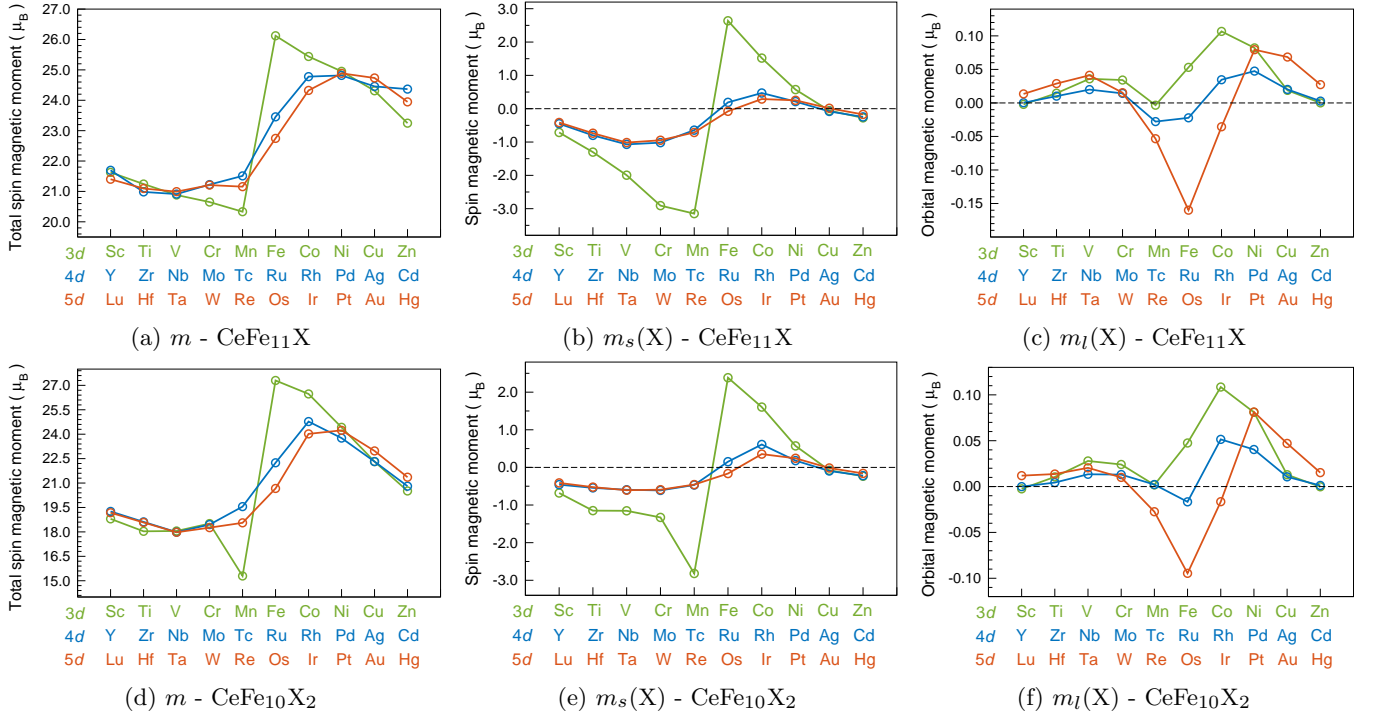


FIG. 6: The magnetic moments of CeFe_{11}X and $\text{CeFe}_{10}\text{X}_2$ systems calculated for various 3d, 4d, and 5d transition metals. (a, d) Total magnetic moments per formula unit and (b, c, e, f) spin and orbital magnetic moments on dopant element X. The calculations were performed with FPLO18 using the PBE functional for quantization axis [010] (easy axis).

increase in magnetocrystalline anisotropy energy (MAE) and magnetic hardness. Using the fully relativistic fixed spin moment method, we calculated for $\text{CeFe}_{11}\text{Ti}$ the dependence of the MAE on the spin magnetic moment, which confirmed the expected relationship that the MAE increases as the magnetic moment decreases.

Almost identical dependence of the anisotropy energy on the magnetic moment as for $\text{CeFe}_{11}\text{Ti}$ was observed for the parent compound CeFe_{12} . We have also shown that the discussed relation of the anisotropy energy on the magnetic moment practically does not depend on the choice of exchange-correlation potential. On the other hand, the equilibrium magnetic moment values obtained depend very strongly on the choice of exchange-correlation potential, which indirectly affects the anisotropy energy values and leads to a very wide spectrum of results, from strongly negative to strongly positive. Additional calculations for CeFe_{12} - and $\text{CeFe}_{11}\text{Ti}$ -based alloys with smaller elements such as B, C, and N placed in interstitial positions showed that such doping can lead to a decrease in the total magnetic moment and an accompanying increase in the MAE.

After a detailed analysis of the structure model of $\text{CeFe}_{11}\text{Ti}$ and verification of the fixed spin moment method, we performed systematic calculations for CeFe_{11}X and $\text{CeFe}_{10}\text{X}_2$ compounds considering a full range of transition metal dopants. We have presented and discussed the courses of dependence of magnetic mo-

ments and magnetocrystalline anisotropy energy on the type of dopant element. The compositions showing very high magnetic hardness include CeFe_{11}W , $\text{CeFe}_{10}\text{W}_2$, $\text{CeFe}_{11}\text{Mn}$, $\text{CeFe}_{10}\text{Mn}_2$, $\text{CeFe}_{11}\text{Mo}$, $\text{CeFe}_{10}\text{Mo}_2$, and $\text{CeFe}_{10}\text{Nb}_2$.

Furthermore, we also determined the effect of 4f electrons on the obtained MAE values by performing $\text{MAE}(m_S)$ calculations for isostructural LaFe_{12} and equilibrium calculations of $\text{LaFe}_{11}\text{Ti}$ and $\text{LaFe}_{10}\text{W}_2$ compounds with an empty 4f shell. By comparing the obtained results for the corresponding systems with Ce, we found a secondary effect of the 4f shell on the MAE value in these systems.

ACKNOWLEDGMENTS

We acknowledge the financial support of the National Science Center Poland under the decision DEC-2019/35/O/ST5/02980 (PRELUDIUM-BIS 1) and DEC-2018/30/E/ST3/00267 (SONATA-BIS 8). We thank Paweł Leśniak and Daniel Depcik for compiling the scientific software and administration of the computing cluster at the Institute of Molecular Physics, Polish Academy of Sciences.

APPENDIX

We present Tables VIII and IX showing the lattice parameters and atomic positions of the considered "1-

11-1" and "1-10-2" systems, and the CeFe_{12} compound. The presented parameters relate directly to the crystallographic structures presented in Figs.1b and 3. The structures shown in Table IX were applied in this work.

-
- [1] Y. Toga, M. Nishino, S. Miyashita, T. Miyake, and A. Sakuma, Anisotropy of exchange stiffness based on atomic-scale magnetic properties in the rare-earth permanent magnet $\text{Nd}_2\text{Fe}_{14}\text{B}$, *Phys. Rev. B* **98**, 054418 (2018).
- [2] B. Das, R. Choudhary, R. Skomski, B. Balasubramanian, A. K. Pathak, D. Paudyal, and D. J. Sellmyer, Anisotropy and orbital moment in Sm-Co permanent magnets, *Phys. Rev. B* **100**, 024419 (2019).
- [3] K. Bourzac, The rare-earth crisis, *Techn. Rev.* **114**, 58 (2011).
- [4] D. Niarchos, G. Giannopoulos, M. Gjoka, C. Sarafidis, V. Psycharis, J. Rusz, A. Edström, O. Eriksson, P. Toson, J. Fidler, E. Anagnostopoulou, U. Sanyal, F. Ott, L.-M. Lacroix, G. Viau, C. Bran, M. Vazquez, L. Reichel, L. Schultz, and S. Fähler, Toward Rare-Earth-Free Permanent Magnets: A Combinatorial Approach Exploiting the Possibilities of Modeling, Shape Anisotropy in Elongated Nanoparticles, and Combinatorial Thin-Film Approach, *JOM J. Miner. Met. Mater. Soc.* **67**, 1318 (2015).
- [5] S. Hirosawa, Current Status of Research and Development toward Permanent Magnets Free from Critical Elements, *J. Magn. Soc. Jpn.* **39**, 85 (2015).
- [6] D. Li, D. Pan, S. Li, and Z. Zhang, Recent developments of rare-earth-free hard-magnetic materials, *Sci. China Phys. Mech. Astron.* **59**, 617501 (2015).
- [7] S. Hirosawa, M. Nishino, and S. Miyashita, Perspectives for high-performance permanent magnets: Applications, coercivity, and new materials, *Adv. Nat. Sci. Nanosci. Nanotechnol.* **8**, 013002 (2017).
- [8] R. Skomski and J. Coey, Magnetic anisotropy — How much is enough for a permanent magnet?, *Scr. Mater.* **112**, 3 (2016).
- [9] S. Ener, K. P. Skokov, D. Palanisamy, T. Devillers, J. Fischbacher, G. G. Eslava, F. Maccari, L. Schäfer, L. V. B. Diop, I. Radulov, B. Gault, G. Hrkac, N. M. Dempsey, T. Schrefl, D. Raabe, and O. Gutfleisch, Twins — A weak link in the magnetic hardening of ThMn_{12} -type permanent magnets, *Acta Mater.* , 116968 (2021).
- [10] M. Werwiński and W. Marciniak, Ab initio study of magnetocrystalline anisotropy, magnetostriction, and Fermi surface of L1_0 FeNi (tetrataenite), *J. Phys. D: Appl. Phys.* **50**, 495008 (2017).
- [11] O. Gutfleisch, M. A. Willard, E. Brück, C. H. Chen, S. G. Sankar, and J. P. Liu, Magnetic Materials and Devices for the 21st Century: Stronger, Lighter, and More Energy Efficient, *Adv. Mater.* **23**, 821 (2011).
- [12] P. Delange, S. Biermann, T. Miyake, and L. Pourovskii, Crystal-field splittings in rare-earth-based hard magnets: An ab initio approach, *Phys. Rev. B* **96**, 155132 (2017).
- [13] H. İ. Sözen, S. Ener, F. Maccari, K. P. Skokov, O. Gutfleisch, F. Körmann, J. Neugebauer, and T. Hickel, Ab initio phase stabilities of Ce-based hard magnetic materials and comparison with experimental phase diagrams, *Phys. Rev. Mater.* **3**, 084407 (2019).
- [14] C. Zhou and F. E. Pinkerton, Magnetic hardening of $\text{CeFe}_{12-x}\text{Mo}_x$ and the effect of nitrogenation, *J. Alloys Compd.* **583**, 345 (2014).
- [15] G. Hadjipanayis, A. Gabay, A. Schönhöbel, A. Martín-Cid, J. Barandiaran, and D. Niarchos, ThMn_{12} -Type Alloys for Permanent Magnets, *Engineering* **6**, 141 (2020).
- [16] Q. Pan, Z.-X. Liu, and Y.-C. Yang, Structural and magnetic properties of $\text{Ce}(\text{Fe},\text{M})_{12}\text{N}_x$ interstitial compounds, $\text{M}=\text{Ti}, \text{V}, \text{Cr}, \text{and Mo}$, *J. Appl. Phys.* **76**, 6728 (1994).
- [17] M. Akayama, H. Fujii, K. Yamamoto, and K. Tatami, Physical properties of nitrogenated RFe_{11}Ti intermetallic compounds ($\text{R}=\text{Ce}, \text{Pr}$ and Nd) with ThMn_{12} -type structure, *J. Magn. Mater.* **130**, 99 (1994).
- [18] L. Ke and D. D. Johnson, Intrinsic magnetic properties in $\text{R}(\text{Fe}_{1-x}\text{Co}_x)_{11}\text{Ti}$ ($\text{R}=\text{Y}$ and Ce ; $\text{Z}=\text{H}, \text{C}$, and N), *Phys. Rev. B* **94**, 024423 (2016).
- [19] R. Martinez-Casado, A. Dasmahapatra, M. F. Sgroi, C. Romero-Muñiz, H. C. Herper, O. Y. Vekilova, A. M. Ferrari, D. Pullini, J. Desmarais, and L. Maschio, The $\text{CeFe}_{11}\text{Ti}$ permanent magnet: A closer look at the microstructure of the compound, *J. Phys.: Condens. Matter* **31**, 505505 (2019).
- [20] O. Isnard, S. Miraglia, M. Guillot, and D. Fruchart, Hydrogen effects on the magnetic properties of RFe_{11}Ti compounds, *J. Alloys Compd.* **275-277**, 637 (1998).
- [21] K. Koepernik and H. Eschrig, Full-potential nonorthogonal local-orbital minimum-basis band-structure scheme, *Phys. Rev. B* **59**, 1743 (1999).
- [22] J. P. Perdew, K. Burke, and M. Ernzerhof, Generalized Gradient Approximation Made Simple, *Phys. Rev. Lett.* **77**, 3865 (1996).
- [23] U. von Barth and L. Hedin, A local exchange-correlation potential for the spin polarized case. i, *J. Phys. C: Solid State Phys.* **5**, 1629 (1972).
- [24] J. P. Perdew and A. Zunger, Self-interaction correction to density-functional approximations for many-electron systems, *Phys. Rev. B* **23**, 5048 (1981).
- [25] J. P. Perdew and Y. Wang, Accurate and simple analytic representation of the electron-gas correlation energy, *Phys. Rev. B* **45**, 13244 (1992).
- [26] A. Edström, M. Werwiński, D. Iuşan, J. Rusz, O. Eriksson, K. P. Skokov, I. A. Radulov, S. Ener, M. D. Kuz'min, J. Hong, M. Fries, D. Y. Karpenkov, O. Gutfleisch, P. Toson, and J. Fidler, Magnetic properties of $(\text{Fe}_{1-x}\text{Co}_x)_2\text{B}$ alloys and the effect of doping by 5d elements, *Phys. Rev. B* **92**, 174413 (2015).
- [27] M. Werwiński, A. Edström, J. Rusz, D. Hedlund, K. Gunnarsson, P. Svedlindh, J. Cedervall, and M. Sahlberg, Magnetocrystalline anisotropy of Fe_5PB_2 and its alloys with Co and 5d elements: A combined first-principles and experimental study, *Phys. Rev. B* **98**, 214431 (2018).
- [28] K. Momma and F. Izumi, *VESTA* : A three-dimensional visualization system for electronic and structural analy-

TABLE VIII: Lattice parameters (in Å) and atomic positions for several considered crystal structures of CeFe₁₁Ti with space groups *Amm*2 (No. 38), *Ama*2 (No. 40), *Imm*2 (No. 44), and *Pmmm* (No. 47). See Fig. 3 for illustrations of the structures.

<i>Amm</i> 2				<i>Ama</i> 2				<i>Imm</i> 2				<i>Pmmm</i>			
<i>a, b, c</i>	4.78	12.075	12.075	<i>a, b, c</i>	4.78	12.075	12.075	<i>a, b, c</i>	4.78	8.539	8.539	<i>a, b, c</i>	8.539	8.539	4.78
site	<i>x</i>	<i>y</i>	<i>z</i>	site	<i>x</i>	<i>y</i>	<i>z</i>	site	<i>x</i>	<i>y</i>	<i>z</i>	site	<i>x</i>	<i>y</i>	<i>z</i>
Ce	0	0	0	Ce	0.25	0.75	0.25	Ce	0	0	0	Ce	0.5	0.5	0.5
Ce	0.5	0.5	0	Fe	0.5	0.25	0	Fe	0.75	0.75	0.0025	Ce	0	0	0
Fe	0.25	0.75	0	Fe	0.5	0.5	0.25	Fe	0	0.64	0	Fe	0.75	0.75	0.75
Fe	0.25	0.5	0.25	Fe	0.5	0	0.25	Fe	0	0	0.36	Fe	0.5	0.14	0.5
Fe	0.25	0	0.25	Fe	0.25	0.93	0.07	Fe	0.5	0	0.235	Fe	0.36	0	0
Fe	0	0.32	0.32	Fe	0.25	0.57	0.07	Fe	0	0.5	0.265	Fe	0	0.36	0
Fe	0.5	0.32	0.18	Fe	0.25	0.57	0.43	Fe	0	0.265	0.5	Fe	0.765	0	0.5
Fe	0.5	0.18	0.32	Fe	0.25	0.1325	0.1325	Ti	0	0	0.64	Fe	0	0.765	0.5
Fe	0	0.1175	0.3825	Fe	0.25	0.3675	0.3675					Fe	0.265	0.5	0
Fe	0	0.3825	0.1175	Fe	0.25	0.3675	0.1325					Fe	0.5	0.265	0
Fe	0.5	0.6175	0.3825	Fe	0.25	0.1325	0.3675					Ti	0.86	0.5	0.5
Fe	0.5	0.8825	0.1175	Ti	0.25	0.93	0.43								
Ti	0	0.82	0.18												

TABLE IX: Lattice parameters (in Å) and atomic positions for CeFe₁₀X₂ (s.g. *P4/mmm*, No. 123), CeFe₁₁Ti (s.g. *Pmmm*, No. 59), CeFe₁₂ (s.g. *I4/mmm*, No. 139). See Fig. 3 for illustrations of the structures.

CeFe ₁₀ X ₂ s.g. <i>P4/mmm</i>				CeFe ₁₁ Ti s.g. <i>Pmmm</i>				CeFe ₁₂ s.g. <i>I4/mmm</i>			
<i>a, b, c</i>	8.539	8.539	4.78	<i>a, b, c</i>	8.539	4.78	8.539	<i>a, b, c</i>	8.539	8.539	4.78
Site	<i>x</i>	<i>y</i>	<i>z</i>	Site	<i>x</i>	<i>y</i>	<i>z</i>	Site	<i>x</i>	<i>y</i>	<i>z</i>
Ce	0.0	0.0	0.0	Ce	0.25	0.25	0.25	Ce	0.0	0.0	0.0
Ce	-0.5	-0.5	-0.5	Fe	0.5	0.5	0.5	Fe	0.3582	0.0	0.0
Fe	0.251	0.251	0.254	Fe	0.5	0.5	0.0	Fe	-0.2275	0.0	0.5
Ti	0.349	0.0	0.0	Fe	0.89	0.25	0.25	Fe	-0.25	0.25	0.25
Fe	-0.141	-0.5	-0.5	Fe	0.25	0.25	0.89				
Fe	0.277	-0.5	0.0	Fe	0.75	0.25	0.515				
Fe	-0.219	0.0	-0.5	Fe	0.75	0.25	0.985				
				Fe	0.515	0.25	0.75				
				Ti	0.25	0.25	0.61				

- sis, J. Appl. Crystallogr. **41**, 653 (2008).
- [29] K. Schwarz and P. Mohn, Itinerant metamagnetism in YCo₂, J. Phys. F: Met. Phys. **14**, L129 (1984).
- [30] P. Nieves, S. Arapan, J. Maudes-Raedo, R. Marticorena-Sánchez, N. L. Del Brío, A. Kovacs, C. Echevarria-Bonet, D. Salazar, J. Weischenberg, H. Zhang, O. Y. Vekilova, R. Serrano-López, J. M. Barandiaran, K. Skokov, O. Gutfleisch, O. Eriksson, H. C. Herper, T. Schrefl, and S. Cuesta-López, Database of novel magnetic materials for high-performance permanent magnet development, Comput. Mater. Sci. **168**, 188 (2019).
- [31] A. Galler, S. Ener, F. Maccari, I. Dirba, K. P. Skokov, O. Gutfleisch, S. Biermann, and L. V. Pourovskii, Intrinsically weak magnetic anisotropy of cerium in potential hard-magnetic intermetallics, npj Quantum Mater. **6**, 2 (2021).
- [32] Y. Harashima, K. Terakura, H. Kino, S. Ishibashi, and T. Miyake, First-principles study on stability and magnetism of NdFe₁₁M and NdFe₁₁MN for M=Ti, V, Cr, Mn, Fe, Co, Ni, Cu, Zn, J. Appl. Phys. **120**, 203904 (2016).
- [33] H. Akai, Nuclear spin-lattice relaxation of impurities in ferromagnetic iron, Hyperfine Interact. **43**, 253 (1988).
- [34] P. H. Dederichs, R. Zeller, H. Akai, and H. Ebert, Ab-initio calculations of the electronic structure of impurities and alloys of ferromagnetic transition metals, J. Magn. Magn. Mater. **100**, 241 (1991).
- [35] R. Wienke, G. Schütz, and H. Ebert, Determination of local magnetic moments of 5d impurities in Fe detected via spin-dependent absorption, J. Appl. Phys. **69**, 6147 (1991).
- [36] M. I. Bartashevich, T. Goto, R. J. Radwanski, and A. V. Korolyov, Magnetic anisotropy and high-field magnetization process of CeCo₅, J. Magn. Magn. Mater. **131**, 61 (1994).
- [37] T. W. Capehart, R. K. Mishra, G. P. Meisner, C. D. Fuerst, and J. F. Herbst, Steric variation of the cerium valence in Ce₂Fe₁₄B and related compounds, Appl. Phys. Lett. **63**, 3642 (1993).